Fly-Inspired Visual Steering of an Ultralight Indoor Aircraft

Jean-Christophe Zufferey, *Member, IEEE,* and Dario Floreano, *Member, IEEE*

***Abstract*—We aim at developing autonomous microflyers capable of navigating within houses or small indoor environments using vision as the principal source of information. Due to severe weight and energy constraints, inspiration is taken from the fly for the selection of sensors, for signal processing, and for the control strategy. The current 30-g prototype is capable of autonomous steering in a 16 × 16 m textured environment. This paper describes models and algorithms which allow for efficient course stabilization and collision avoidance using optic flow and inertial information.**

***Index Terms*—Collision avoidance, indoor flying robot, optic flow (OF), steering control.**

I. Introduction

THIS paper describes a 30-g airplane capable of autonomous steering and collision avoidance in a 16×16 m experimental room using only visual and inertial information. It represents a major step toward our goal of developing autonomous microflyers capable of navigating within houses or small indoor environments. Flying indoors involves a number of challenges, such as small size and slow speed for maneuverability, light weight to stay airborne, low-power electronics, and smart sensing and control to fly in cluttered environments. One of the main issues when developing such a small flying device is that sensors commonly employed in robotics, in particular, active range finders, are too heavy and energy-consuming to match the limited payload (less than 10 g) of an indoor aircraft. Efficient flight control under drastic weight and energy constraints is an issue that is successfully solved by flying insects like flies. Therefore, we take inspiration from these remarkable and well-studied biological systems for the selection of sensory modalities and design of navigational strategies.

The fly's primary sensor for flight control consists of two compound eyes that span an almost omnidirectional field of view (FOV) with coarse resolution [2]. Their optic lobes contain motion-sensitive neurons which respond to retinal image shifts, the so-called optic flow (OF), induced by the motion of the eyes relative to the surroundings [3]. The fly has several OF-sensitive neurons that have been linked to specific visually guided behaviors (for a review, see [4]). OF is a linear combination of two components, one resulting from rotation (RotOF) and one from translation (TransOF). TransOF is the only component that depends on the distance from an object [5]. If the RotOF component can be cancelled, OF provides useful information for tasks related to depth perception, such as collision avoidance. This may be the reason why flies navigate using a series of straight segments separated by rapid turns, known as saccades [6], [7]. Straight trajectories allow them to experience pure TransOF, which they use to decide when to initiate a saccade. During saccades, flies seem to ignore the visual information, which is dominated by the RotOF component. Flies also possess sensitive mechanosensory structures, called halteres, that detect rotations of the body, allowing them to maintain equilibrium in flight [8]. The working principle of these biological sensors resembles micro-electro-mechanical systems (MEMS) piezo-electric rate gyros, which sense Coriolis forces that act on oscillating mechanical parts. Halteres have also been shown to play an important role in gaze stabilization [9], which may serve to cancel residual RotOF due to turbulence while flying on a straight trajectory.

The design of our autonomous microflyer takes inspiration from the fly's characteristics at three levels. At the sensory level, the flying robot is equipped only with low-resolution visual sensors and a MEMS rate gyro. At the signal processing level, it estimates OF and fuses it with inertial information in order to provide the control system with the same kind of signals used by flies. At the behavioral level, the control system is designed to produce straight trajectories interspersed with fast turning actions when imminent collision is detected by the visual system.

The rest of this paper is organized as follows. After a short overview in Section II of related projects on miniature aerial robotics and bioinspired vision-based navigation, Section III describes our 30-g flying platform and its electronic equipment. Section IV gives the implementation details of the lightweight OF detectors on this aircraft. Section V outlines the control strategy inspired from biological models, and Section VI presents the results obtained in flight. At the end is a final discussion and a few ideas about future work.

II. Related Work

A. Bioinspired Vision-Based Navigation on Wheels

Several bioinspired strategies for vision-based navigation have been developed on wheeled robots for obstacle avoidance [10]–[13] or corridor following [14]–[17]. However, most of those systems either use wheel encoders, or, more generally, their contact with the ground to reduce interference from RotOF and/or implement active gaze stabilization. With small

Manuscript received November 12, 2004; revised April 11, 2005. This paper was recommended for publication by Associate Editor G. Sukhatme and Editor F. Park upon evaluation of the reviewers' comments. This work was supported by the Swiss National Science Foundation. This paper was presented in part at the IEEE International Conference on Robotics and Automation, Barcelona, Spain, 2005.

The authors are with the Ecole Polytechnique Fédérale de Lausanne (EPFL), Laboratory of Intelligent Systems, CH-1015 Lausanne, Switzerland (e-mail: jean-christophe.zufferey@epfl.ch; dario.floreano@epfl.ch).

Digital Object Identifier 10.1109/TRO.2005.858857

flying robots, it is, of course, not possible to rely on wheel encoders, and the tight weight budget excludes the use of mobile cameras. Most of the above-mentioned robots, except the one by Franceschini and colleagues [10], rely on off-board image processing and control. Recently, we proposed a set of vision-based control strategies enabling collision avoidance and altitude control [1], [18]. Those control strategies were tested on a small wheeled robot equipped with electronic components very similar to those used on the 30-g aircraft described here. Image processing and control were fully implemented in the onboard 8-b microcontroller, paving the way toward fully autonomous indoor microflyers.

B. Bioinspired Micromechanical Flying Robots

Other projects have aimed at developing ultralight, unconventional micro flying machines with centimeter-scale rotors [19] or flapping wings [20], [21]. Although those devices represent a remarkable micromechatronic challenge, none of them are yet capable of autonomous navigation; neither are they equipped with exteroceptive sensors.

In an even smaller scale, R. Fearings' team is currently attempting to create a micro flying robot that replicates the wing mechanics and dynamics of flies [22]. The expected weight of the final device is approximately 100 mg for a 25-mm wingspan. So far, a single wing on a test rig, linked to an off-board power supply, has generated about 0.5 mN average lift [23]. The team is currently working on a biomimetic sensor suite for attitude control [24], [25], but in-flight tests have not yet been reported.

In our project, we opted for a more classical flying scheme (an airplane), in order to be able to concentrate on control strategy and navigational autonomy, rather than micromechanical developments and aerodynamic studies. However, in order to reasonably maneuver indoors, a flying robot should be able to fly around 1 m/s and have a minimum turning radius of about 1 m. Therefore, a significant effort has been made to optimize wing profile and minimize the weight of the airframe and the actuators in order to reduce the wing loading as much as possible, thereby minimizing stall speed and improving maneuverability [26].

C. Bioinspired Vision-Based Aerial Navigation

Specific studies on insect-inspired altitude control have been conducted in simulation [27], with tethered helicopters [28], and with outdoor unmanned air vehicles [29]. Full 3-D navigation (attitude control, obstacle avoidance, course stabilization, and altitude control) using OF has been demonstrated in simulation [30]. In that case, the dynamics of the simulated agent was based on a minimalist model of an insect without inertia or detailed aerodynamics. Another work with a simulated helicopter showed efficient navigation and obstacle avoidance in urban canyons using high-resolution, 2-D OF and inertial measurements [31]. Experiments of fly-inspired guidance have also been carried out on a robotic gantry [32], successfully demonstrating an artificial implementation of a model of the fly's visual system for autonomous steering. Although these studies on simulated or tethered robots are important proofs of concept, they cannot totally replace experiments on free-flying devices, which generally have more uncontrolled parameters and richer dynamics.

Experiments about obstacle avoidance and altitude control have been carried out by Centeye (Washington, DC) with hobbyist model planes equipped with mixed-mode very large scale integration (VLSI) OF detectors [33], [34]. Building upon this preliminary work, Oh *et al.* were the first to demonstrate autonomous landing [35] and collision avoidance [36] with lightweight, fixed-wing aircrafts in indoor environments [37]. For each experiment, the flying robot was equipped with only one 1-D OF detector from Centeye so that it could either act on the pitch angle while looking downward, or steer away from obstacles occurring on one side by looking either right or left. No inertial sensors were used, and the RotOF component was assumed to be small, but it is unclear whether this was actually the case. The flying robot was not equipped with wireless communication capabilities, therefore, no data could be logged during flight tests and no *a posteriori* analysis was possible. Those experiments were carried out in unchanged indoor environments (usually basketball courts), but no continuous autonomous flight has been reported so far. The only data available is video recordings of, for example, one-shot avoidance of a basketball basket in front of an otherwise uniform background.

In our experiment, we focus on control strategy for continuous autonomous steering in an enclosed environment of 16×16 m. The goal is not yet to develop adaptive OF detectors capable of providing reliable data in the presence of strongly varying visual characteristics (background light, contrast, spatial frequency). Therefore, we are using very simple, commercially available cameras as the visual sensor front-end. Since those cameras are not very sensitive, the experimental arena is equipped with high contrast textures on the walls. The 30-g airplane has two 1-D OF detectors, such that it can symmetrically avoid frontal and lateral obstacles on both sides while actively deciding the optimum direction of the avoidance maneuver. Inertial measurements are used to enhance OF signals by cancelling RotOF generated by turbulence or corrective rudder actions. Finally, a wireless communication device allows for plotting sensory data for *a posteriori* analysis.

III. Flying Platform

A. Airframe

The current version of our microflyer (Fig. 1) is made of carbon-fiber rods and balsa wood for the frame, and thin plastic film (2.2 g/m^2) for the lifting surfaces. It is propelled by a miniature 6-mm DC motor with a gearbox driving a balsa-wood propeller. Two miniature servos from Didel (Belmont/Lausanne, Switzerland) are placed at the back end of the fuselage to control the rudder and elevator. The plane has a wingspan of 86 cm. Table I gives an overview of the weight distribution for the configuration used in the experiment described in this paper.

The speed range during flight lies between 1.2–2.5 m/s, and its yaw rotation speed is in the range $\pm 100°$/s. At 2 m/s flight speed, the curvature radius can be less than 1.3 m. This aircraft has no ailerons on the wings. It uses its vertical rudder to steer. This is sufficient, since yaw motion is highly coupled with roll

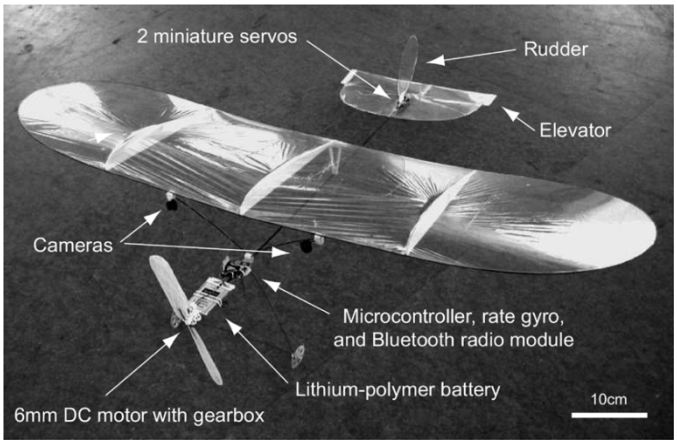

Fig. 1. 30-g aircraft with description of electronic components, sensors, and actuators.

Fig. 2. Experimental room measures 16×16 m and is equipped with contrasting walls made of black and white curtains. Note that the regularity of the pattern is due to the default size of the material from the store.

TABLE I
WEIGHT DISTRIBUTION OF THE 30-G AIRPLANE

Fuselage and tail	:	4.7g
Wing	:	4.5g
Landing gear	:	1.2g
Motor, gearbox, propeller	:	2.7g
Two servos	:	2.7g
Battery	:	6.9g
Electronic board with gyroscope and radio	:	4.0g
Two cameras	:	2.2g
Miscellaneous (cables, glue)	:	1.1g

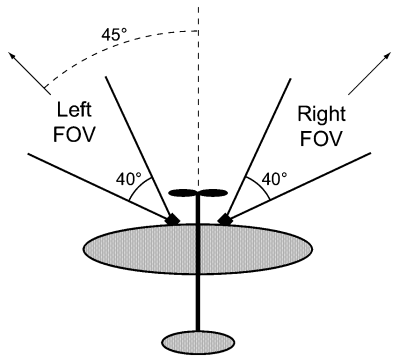

Fig. 3. Top view of the airplane with superposition of orientation and FOV of the 1-D cameras.

rotation, so that rudder deflection on the left provokes a leftward roll resulting in a leftward turn. Moreover, the small angle appearing between the left and right wings when the plane is aloft (the wing bends upward due to aerodynamic lift) provides passive roll stability (this is known as the dihedral effect in aerodynamics), so that when the rudder is in its neutral position, the plane tends to cancel any bank and comes back to horizontal automatically after a few seconds.

Due to its very low inertia, this lightweight aircraft is seldom damaged when crashing into obstacles, which is useful during the parameter-tuning phase. In order to further limit the risk of damaging the aircraft during development of the control strategies, the experimental room was covered with black and white curtains that also provided visual texture (Fig. 2).

B. Electronics

The custom-designed embedded electronic board features an 8-b microcontroller running at 20 MHz (Microchip (Chandler, AZ) PIC18F6720, 3840 B of RAM, 64 kwords of program memory) for vision processing and control, a MEMS piezoelectric rate gyro (AnalogDevices (Norwood, MA) ADXRS150, angular velocity range 150°/s) for yaw rotation, and a Bluetooth module (Mitsumi (Tokyo, Japan) WML-C10-AHR) for bidirectional communication with a ground station. On-board energy is provided by a 310 mAh lithium-polymer battery. The power consumption of the electronics (including wireless communication) is about 300 mW, whereas overall peak consumption reaches 2 W. The in-flight average consumption allows for an energetic autonomy of about 30 min.

C. Vision System

The choice of a suitable vision system for such an aircraft is not trivial. On the one hand, it is well known that motion fields spanning wide FOV are easier to interpret [38], and indeed, nearly omnidirectional vision is a characteristic feature of most flying insects, which possess wide-field, motion-sensitive neurons [39]. On the other hand, artificial vision systems with wide FOV are likely to be too heavy for our application, because they need either a special mirror or fish-eye optics with multiple glass lenses. Such subsystems would also require too much processing power from the onboard microcontroller, which should grab 2-D images and process them in real time. The tradeoff we adopted consists of using multiple lightweight 1-D cameras. The underlying idea is that several of these restricted FOV cameras can be mounted on the aerial robot in order to look in specific directions (see Section V-A) according to the particular task to be solved, while maintaining the total weight and computational requirements within the limits of the aircraft. For the collision-avoidance experiment described here, we use only two horizontal cameras oriented at 45° off the longitudinal axis of the plane (Fig. 3). Those cameras (TAOS (Plano, TX) TSL3301) feature a 1-D array of 102 grey-level pixels, out of which only 28 pixels in the middle are used for the OF detection, and a horizontal FOV of about 40° (see [40] for further details on this camera, possible optics, and comparison with other vision systems).

IV. Optic Flow Detection

A. Algorithm

In order to measure OF with the onboard microcontroller, we adapted the image interpolation algorithm (I2A) proposed by Srinivasan [41], which estimates the global motion in a given region of the image by a single-stage, noniterative process. This algorithm computes the displacement s that provides the best fit between a linear combination of two shifted versions of a reference image and a new image acquired after a small delay $\triangle T$. The ratio $s/\triangle T$ (in pixel/s) is proportional to the actual OF (in °/s), and $\triangle T$ can be used as a parameter to scale the OF output (see Section IV-B).

The algorithm, which has been adapted to 1-D images, works as follows. Let $I(n)$ denote the grey level of the nth pixel in the 1-D image array. The algorithm computes the amplitude of the translation s between an image (or a subpart of it) captured at time $t, I_t(n)$, which is called "reference image," and a later image captured at time $t+1, I_{t+1}(n)$. It assumes that, for small displacements of the image, $I_{t+1}(n)$ can be approximated by $\hat{I}_{t+1}(n)$, which is a weighted linear combination of the reference image and of two shifted versions $I_t(n \pm k)$ of that same image

$$\hat{I}_{t+1}(n) = I_t(n) + s\frac{I_t(n-k) - I_t(n+k)}{2k} \tag{1}$$

where k is a small reference shift in pixels. The image displacement s is then computed by minimizing the mean square error E between the estimated image $\hat{I}_{t+1}(n)$ and the new image $I_{t+1}(n)$ with respect to s

$$E = \sum_n [I_{t+1}(n) - \hat{I}_{t+1}(n)]^2 \quad \text{and} \quad \frac{dE}{ds} = 0 \Leftrightarrow \tag{2}$$

$$s = 2k\frac{\sum_n [I_{t+1}(n) - I_t(n)][I_t(n-k) - I_t(n+k)]}{\sum_n [I_t(n-k) - I_t(n+k)]^2}. \tag{3}$$

In our case, the shift amplitude k is set to one pixel, and the delay $\triangle T$ between t and $t+1$ is chosen such to ensure that the actual shift does not exceed ± 1 pixel. $I_t(n \pm 1)$ are thus artificially generated by translating the reference image by one pixel to the left and to the right, respectively. More details about this algorithm, as well as a theoretical assessment of its robustness against different perturbations occurring in real-world conditions, can be found in [18, p. 86].

B. Implementation Issues

Equation (3) has been implemented in the embedded microcontroller and applied separately on images coming from the left and right cameras. The microcontroller grabs two successive images corresponding to the reference image $I_t(n)$ and the new one $I_{t+1}(n)$ with a delay $\triangle T$ of a few milliseconds. Every pixel intensity is encoded on 8 b, and the variables used in (3) are 32-b integers. The computation is performed in fixed point and lasts only 0.9 ms for 28 pixels, whereas grabbing an image takes less than 0.2 ms.

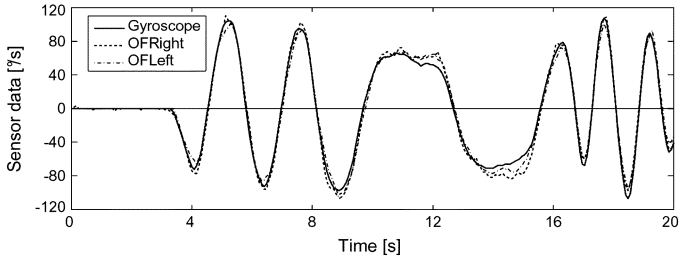

Fig. 4. Match between gyroscopic values and OF estimates of the right (OFRight) and left (OFLeft) OF detectors. The data have been recorded every 80 ms while the plane was held by hand in the experimental arena and randomly rotated around its yaw axis.

The delay $\triangle T$ is adjusted so that the RotOF values match the rate gyro output when the robot undergoes pure yawing rotation. This empirical calibration provides an optimal $\triangle T$ of 6.4 ms. Fig. 4 shows the resulting good match between rotations estimated by the OF detectors and by the rate gyro, while the aircraft is manually rotated about its yaw axis in the experimental arena (Fig. 2).

V. Control Strategy

The control strategy for autonomous steering is largely based on the behavior of the fly. For a long time, biologists have been studying the visual cues that affect steering in free-flying flies [6]. A recent paper by Tammero and Dickinson [7] suggests that OFDiv is responsible for triggering saccades, the direction of the saccades (left or right) is opposite to the side experiencing larger OF, and the saccade does not depend on visual feedback. Similarly, our aircraft flies along straight trajectories interspersed with rapid and short turning actions whose duration is fixed. The purpose of this section is to describe the sensory information and control laws that govern this behavior.

The control strategy can be divided into two states: (A) maintain straight trajectory; (B) turn as quickly as possible. The first one is easily implemented by means of a proportional feedback loop connecting the rate gyro to the rudder servomotor, whereas the second one, i.e., the saccade itself, is programmed as a series of rudder commands of a fixed amount of time (1 s). Vision is only required for initiating the saccade, i.e., for the transition from state (A) to state (B). This transition is based on OF estimates acquired during straight flight and, more precisely, on two criteria described in the following paragraph.

A. Triggering a Saccade

In order to find the typical OF signals that the controller can use to trigger a saccade, let us start by studying typical TransOF patterns as they could be experienced by the plane in three different cases of straight flight at constant forward velocity: (a) perpendicularly approaching a flat wall; (b) approaching a flat wall at 30°; and (c) approaching a corner at 45°. Those situations have been chosen as representative samples of flight in an empty rectangular room. Fig. 5 shows the resulting TransOF fields obtained from the formal description of the

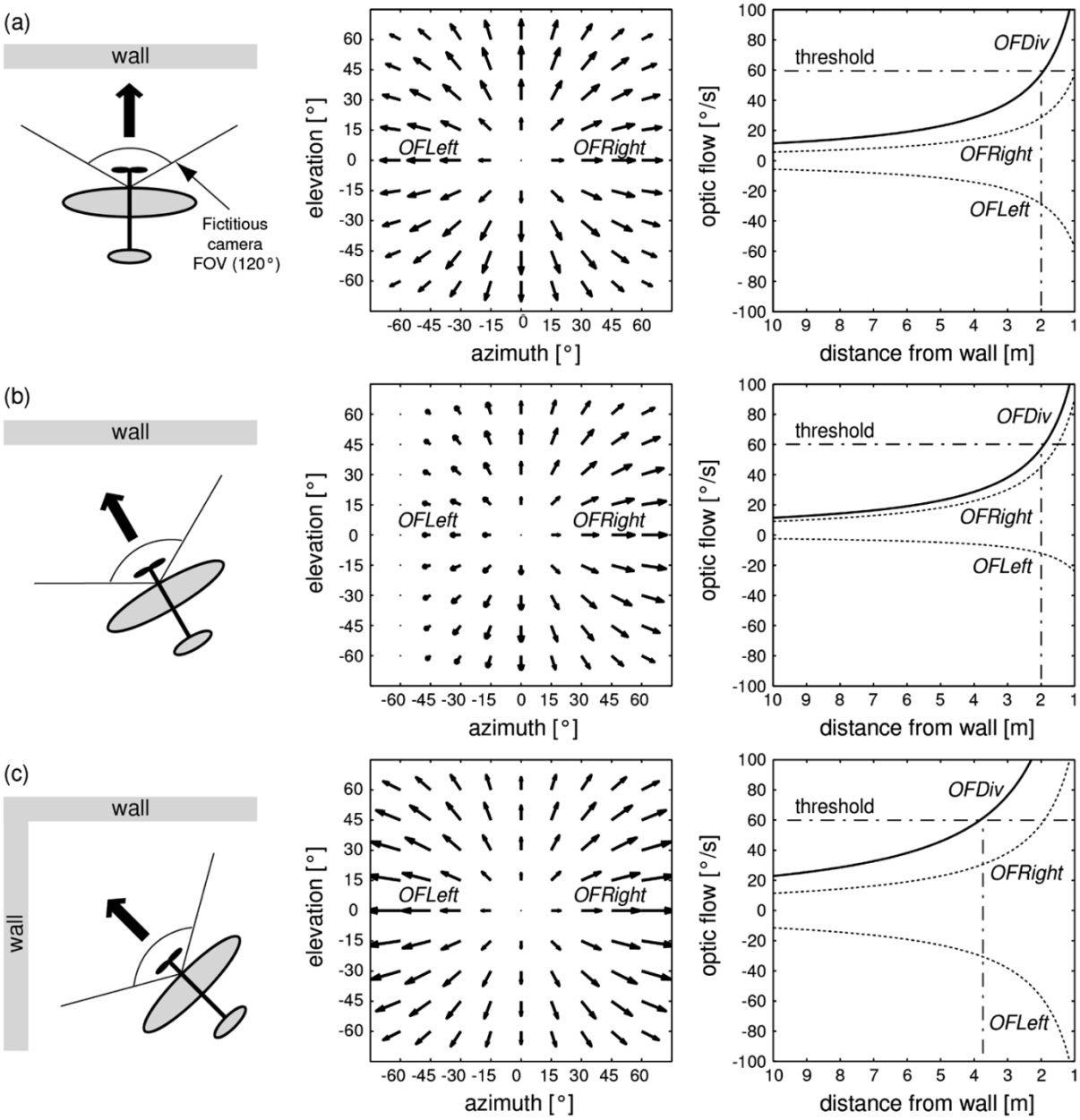

Fig. 5. Ideal motion fields as viewed by a single (fictitious and forward looking) 2-D camera with 120° FOV. (a) Frontal approach toward a wall. (b) Approach at 30°. (c) Approach at 45° to a corner. The first column depicts the fictitious camera position and orientation, as well as the airplane trajectory. In these examples, the aircraft is flying straight at 2 m/s. The second column displays the motion fields occurring in each situation. The third column shows the OF amplitude at 45° azimuth as a function of distance from the wall. OFLeft and OFRight are the OF values measured at $\pm 45^\circ$ azimuth, whereas OFDiv is the sum of OFRight and OFLeft amplitudes, which is a measure of OFDiv, as further explained in the text.

motion field[1] [5]. These fields are based on a fictitious, large FOV, 2-D camera; only portions of these fields are actually covered by the two 1-D cameras present on the robot.

When the plane is flying straight toward a flat surface, the OF field is divergent with an amplitude inversely proportional to the distance, as illustrated in the rightmost graphs of Fig. 5, where two OF signals (OFRight and OFLeft) corresponding to the viewing direction of the plane's cameras ($\pm 45^\circ$ azimuth and zero elevation) are plotted. A measurement of OF divergence (OFDiv) can be obtained by subtracting the values of right and left OF amplitudes (as one can read on the last column curves in Fig. 5)[2]

$$\text{OFDiv} = \text{OFRight - OFLeft.} \tag{4}$$

This information can thus be used to trigger a saccade when OFDiv exceeds a preset threshold (see, for instance, the dashed

[1]In general, a difference is made between motion field and OF. The *motion field* results from pure geometrical considerations and is the 2-D projection onto the retina of a moving eye of the relative 3-D motion of scene points. In opposition, the *OF* is defined as the *apparent* motion of the image, and does not necessarily correspond to the motion field, in particular when no contrast is detectable in a given viewing direction or because of the aperture problem [42]. In this paper, however, we assume enough contrast on the surrounding surfaces such that this distinction can be ignored. In practice, we low-pass filter the OF signal over time, so to limit the impact of losing it during a short period of time.

[2]This way of measuring OFDiv is reminiscent of the minimalist method proposed in [43], using Green's theorem [44].

line at 60°/s corresponding to 2 m from the wall). OFDiv is independent of the angle at which the plane approaches the wall, as can be seen by comparing the curves labeled OFDiv in the first and second rows of Fig. 5. OFDiv is larger when the aircraft happens to fly toward a corner (Fig. 5, third row) because distances from surrounding surfaces are less than the distance from the wall in the heading direction. Therefore, the saccade is triggered farther away than when approaching a flat wall (for instance, the same threshold of 60°/s is reached at more than 3.5 m away), which prevents the plane from going into situations from which it could not easily get out.

The considerations made so far are based on the assumption of constant velocity. It is true that the velocity of the plane will not change abruptly, but one could wonder what would happen if instead of flying at 2 m/s, it slows down to near to the stall speed (1.2 m/s)? It can be shown that TransOF is inversely proportional to the ratio of the distance over the velocity, which is nothing else than the time-to-contact [43], [45], [46]. As a result, even if the forward speed of the flying agent is unknown, OFDiv is proportional to the inverse of the time-to-contact, which means that for a given threshold, the criterion for initiating a saccade will always trigger at the same time before collision. In other words, if the robot moves faster, it will start the saccade farther away from the wall, which is naturally a wise behavior.

In order to decide the direction of the saccade, one can consider another criterion, i.e., the difference between the left and right absolute OF values (OFDiff)

$$\text{OFDiff} = |\text{OFRight}| - |\text{OFLeft}|. \tag{5}$$

A positive OFDiff means a closer obstacle on the right. Since in this case, only the sign of the criterion is taken into account, the velocity of the plane will have no influence.

B. Rotational OF Correction

One of the problems with this approach is that ensuring that there is absolutely no rotation during straight sequences is nearly impossible, because of air turbulence or small yawing movements due to the gyroscope-based heading control. The resulting RotOF component does not contain any information about surrounding distances, and for all kinds of tasks related to distance, a pure translatory OF field is desirable [47]. This holds for the flying robot just as it does for the fly, which is known to compensate with its head for rotations detected by its halteres [9]. Since the small airplane cannot afford to move its cameras with respect to the fuselage, we propose another means of cancelling residual RotOF, based on the same sensory modality used by the fly.

Since the global OF is a linear combination of translatory and rotatory components [5], if one can measure rotation using another sensory modality, it is, in principle, possible to deduce RotOF from the global flow field by simple vector subtraction. In our case, the situation is even simpler, because the OF detection (see Section IV) is 1-D and the rate gyro axis is oriented perpendicular to the pixel array and the viewing directions, reducing the correction operation to a scalar subtraction. Section IV-B further supports this idea by showing the good match between RotOF and rate gyro output in our robot.

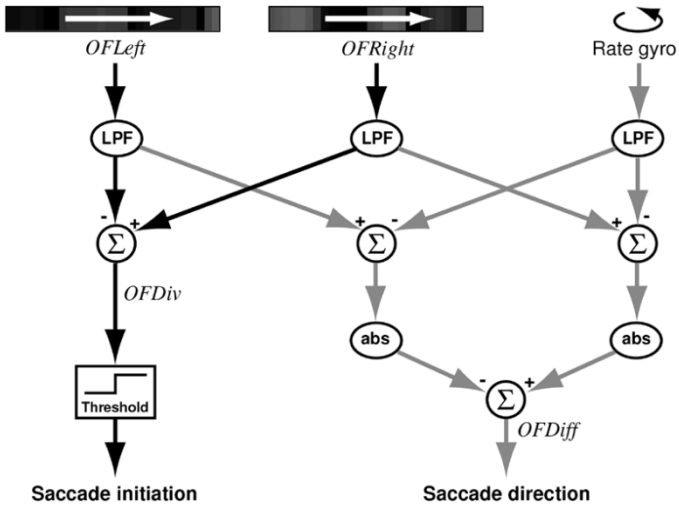

Fig. 6. Signal flow diagram for saccade initiation based on horizontal OFDiv and yaw rotation rate as detected by the gyroscope. "LPF" stands for low-pass filter and "abs" is the absolute value operator.

It is notable, however, that OFDiv, as computed in (4), is not sensitive to yaw rotation. As outlined by Ancona and Poggio [43], this method for computing flow divergence is independent of the location of the focus of expansion (FOE), meaning that even if RotOF due to yaw rotation shifts the FOE, the measured divergence remains unaltered. Unlike OFDiv, OFDiff does suffer from RotOF. As a consequence, it is important, at least for this signal, to discount rotation before computing the criteria in order to decide the saccade direction.

In summary, Fig. 6 gives an overview of the signal flow from sensory input to saccade initiation and direction selection. Temporal leaky integrators are used as a first signal-processing step. Formally equivalent to first-order low-pass filters (LPFs), they also cancel sensory noise. LPFs have equally been proposed as an important component in the model for imminent collision detection in flies [48].

VI. In-Flight Experiment

A. Control Implementation

The sensory-motor cycle lasts 80 ms, during which data from onboard sensors are processed, rudder commands are issued, and significant parameters are sent to a laptop for data logging. About 50% of this sensory-motor cycle is used for wireless communication. OF is processed according to (3), taking data from two images grabbed one after the other at the beginning of every sensory-motor cycle. In other words, OF is estimated once every 80 ms.

During a saccade, whose duration is set to 1 s, the rudder deflection follows an experimentally optimized curve up to full deflection in the direction decided by OFDiff. At the end of the saccade, the plane resumes straight flight while it is still in a banked position. Since a banked posture always produces a yawing motion, the proportional controller based on the rate gyro actively compensates, so as to force the plane back to horizontal. This control strategy is summarized in Fig. 7.

As proposed in the model of the fly by Tammero and Dickinson [7], we implemented an inhibition period after each sac-

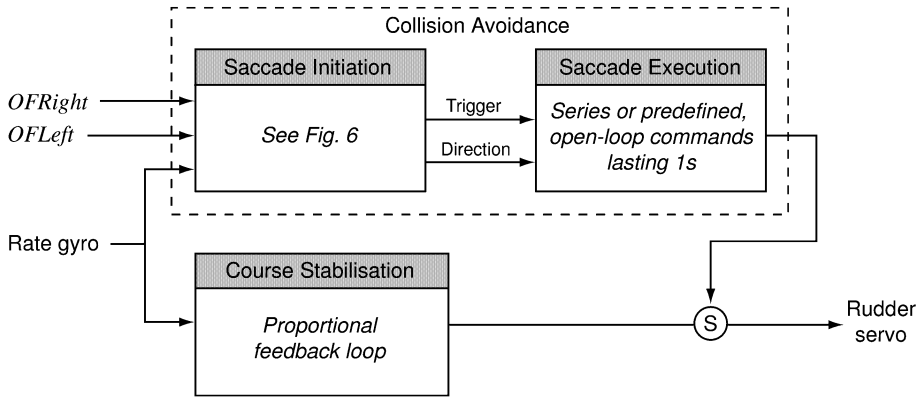

Fig. 7. Overview diagram of the control strategy implementation. On the left are the sensory inputs (OF detectors and gyroscope), and on the right is the system output (the rudder actuator). This diagram is voluntarily inspired from the subsumption architecture proposed by Brooks [49]. The bottom layer accounts for the course stabilization behavior, and the top layer for the collision-avoidance behavior. The encircled "S" represents a suppression node, meaning that, when active, the signal coming from above replaces the signal usually going horizontally through the node.

cade, during which another turning action cannot be triggered. This allows the plane to recover almost straight flight before deciding whether to perform another saccade. In our case, the inhibition lasts as long as the rate gyro indicates an absolute yaw rotational speed larger than 20°/s. This inhibition is to make sure that when active, the OF detectors are providing reliable data and are not noisy due to excessive rotation rate.

B. Experimental Conditions

Autonomous steering experiments have been carried out in the arena depicted in Fig. 2. In addition to natural light coming from outside, the soft walls were lit from the center of the room with eight projectors sitting on the ground.

The Bluetooth radio connection with a ground-based laptop computer was always established in order to log sensor data in real time while the robot is operating. The plane was started manually from the ground by means of a joystick connected to the laptop. When it reached an altitude of about 2 m, the robot was switched into autonomous steering mode. The human pilot has then no access to the rudder (the vertical control surface, shown in Fig. 1), but could modify the pitch angle by means of the elevator (the horizontal control surface). The operator could switch back to manual mode at any moment, if required.

Before testing the plane in autonomous mode, the OFDiv threshold for saccade trigger has been experimentally determined by flying manually in the arena and recording OF signals when frontally approaching a wall until the last possible moment when the pilot had to start an emergency turn. The recorded data could then be analyzed, and the threshold decided on the basis of the value reached by OFDiv just before steering.

C. Results

The 30-g robot was able to fly collision-free in the 16×16 m room for more than 4 min without any intervention regarding its steering.[3] The plane was engaged in turning actions only 20% of the time, which indicates that it flew always in straight trajectories except when very close to a wall. During those 4 min, it covered about 300 m in straight motion and generated 50 saccades.

Fig. 8 displays a detailed 18-s sample of the data acquired during typical autonomous flight. Saccade periods are indicated with vertical gray bars spanning all the graphs. In the first row, the rate gyro provides a good indication of the behavior of the plane, i.e., straight trajectories interspersed with turning actions, in which the plane can reach up to 100°/s. OF is estimated from the 1-D images shown in the second row. The quality of the lightweight imagers and optics does not allow for perfect and noise-free images. As a result, OF estimates (on the two next graphs) are not always very accurate, especially when the plane is close to the walls with a high yaw rotation rate. This situation happens in particular during inhibition periods. Therefore, we set OFDiv and OFDiff (two last rows in Fig. 8) to zero whenever the rate gyro indicates more than 20°/s. When OFDiv reaches the threshold indicated by the dashed line, a saccade is triggered. The direction of the saccade is given by OFDiff, which is plotted on the bottom graph. The first turning action is leftward, because OFDiff is positive when the saccade is triggered. The other ones are rightward because of the negative value of OFDiff.

VII. Discussion

We presented a bioinspired technique enabling autonomous steering and collision avoidance on an ultralight indoor aircraft. Although the primary purpose of this project is to engineer indoor autonomous microflyers, the size, weight, energy, and computational constraints of the robotic platform encouraged us to look at mechanisms and principles of flight control exploited by insects. Bioinspiration has been used at three different levels in order to meet those constraints.

The first level concerns of the type of sensors we decided to employ. Although the fly also possesses hairs or mechanosensors on its neck or wings [50], eyes and halteres are clearly the most important sensors for flight control. Probably because of their inherent complexity and energy consumption, no active distance sensors, like sonar, are present in the fly. The robot's rate gyro can be seen as a close copy of the fly's halteres, although it measures rotation only about one axis, whereas its biological counterpart is known to be sensitive to rotation around

[3]Video clips showing those results can be downloaded from http://phd.zuff.info.

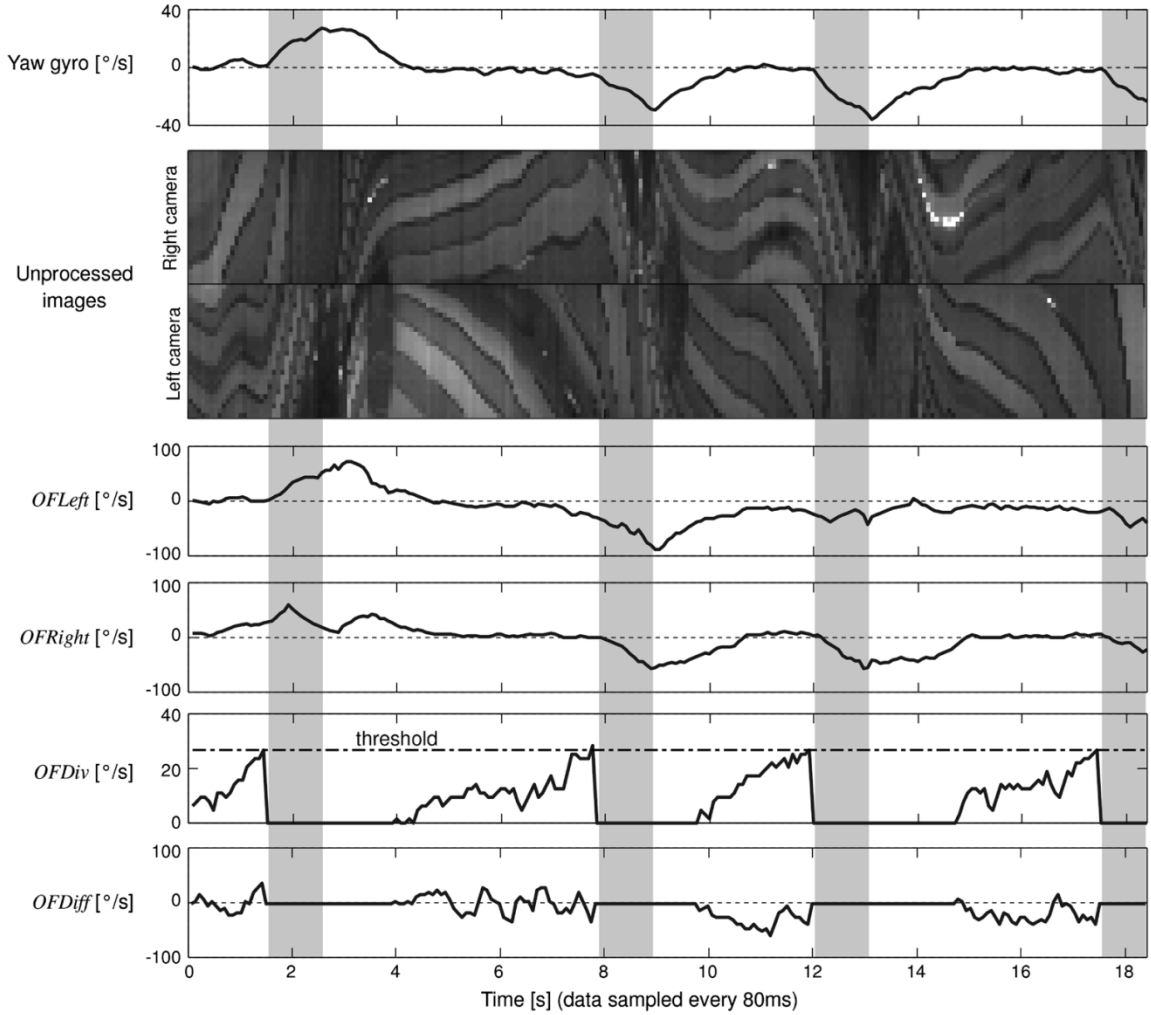

Fig. 8. Sensor and OF data recorded during autonomous flight (about 18 s are displayed). First row is the rate gyro output indicating how much the plane is rotating (leftward positive). The second row displays the raw images (pixels are arranged vertically) grabbed by the two 1-D cameras every sensory-motor cycle. Only the 28 pixels used for OF detection are displayed for each camera. Third and fourth rows are the OF as estimated from the left and the right cameras, respectively. Fifth and sixth rows show OFDiv and OFDiff when absolute value of the rate gyro is below 20°/s, i.e., when the plane is roughly flying straight. The dashed horizontal line in the OFDiv graph represents the threshold for triggering a saccade. The gray vertical lines spanning all the graphs indicate the saccades themselves, i.e., when the turning motor program is in action. The first saccade is leftward and the next three are rightward, as indicated by the rate gyro output in the first column.

all three axes [8]. Notice, however, that a future implementation of altitude regulation is likely to require at least one additional rate gyro. The artificial vision system shares with its biological counterpart a rather low resolution, because its interpixel angle (1.4°) is on the same order of magnitude as the interommatidial angle of most flying insects (1–3°) [2]. The FOV of our airplane is much smaller than that of most flying insects. Although it is sufficient for the simple environment used here, it will have to be expanded for more complex indoor situations.

The second level of bioinspiration concerns the stage of sensor signal processing. Although the extraction of OF itself is not based on correlation-based elementary motion detectors [51] because of their known dependency on contrast and spatial frequency [52], OF is employed as a primary cue in the behavioral control of the airplane, just as it is in the fly [4]. In particular, using looming cues for detecting approaching objects are believed to play a major role in the initiation of saccades [7]. A model explaining the landing reflex of flies has been proposed [48] where the OFDiv signal is integrated over time (with some leakage) until it exceeds a threshold, which finally triggers an action. Although the neuroanatomical details are not yet fully understood, the same model is also employed to explain the initiation of saccades [53]. The attractive feature of this simple scheme is that it does not require explicit measurement of distance or time-to-contact, nor does it rely on accurate knowledge of the flight velocity. This idea has also been stressed by Srinivasan and colleagues [54], who pointed out that it is often possible to achieve efficient behaviors like collision avoidance, landing, corridor following, and altitude control by simply relying on OF values rather than trying to estimate accurate distances. This OF-based approach without explicit estimation of distances has also been used in artificial systems for altitude control and automatic landing [28], [55]. Another example of bioinspired signal processing is the fusion of inertial information with vision. Although the simple scalar summation employed in our robot is probably far from what actually happens in the fly's nervous system, it is clear that some important interactions between visual input and haltere

feedback exist [8]. Recently, a model based on a weighted sum between the two sensory modalities has even been proposed to explain the fly's equilibrium reflex [56].

The third level of bioinspiration concerns trajectory control, where the flight along straight lines interspersed with rapid turning actions is patterned after fly behavior. While in flies, some saccades are spontaneously generated in the absence of any visual input, reconstruction of OF patterns based on flies' motion through an artificial visual landscape suggests that image expansion plays a role in triggering saccades [7]. Aside from providing a first stage of RotOF cancellation, straight flight sequences also increase the quality of visual input by maintaining a horizontal attitude. In addition, straight flight is energetically efficient, because when a plane banks, it has to produce additional lift in order to compensate for the centripetal force. In our implementation, the entire saccade is performed without sensory feedback, whereas flies may continue to rely on sensory input. Although during saccades elementary motion detectors [51] are known to operate beyond their linear range, where the signal could even be reversed because of temporal aliasing [52], whether or not visual feedback plays an important role for controlling these fast turning maneuvers is still under investigation [53]. However, haltere feedback is more likely to have a major impact on the duration of the saccade [8], and integration of the rate gyro output over time could provide a good way of ensuring a given rotation angle independently of the aircraft velocity at the beginning of the saccade. Although the precise roles of halteres and vision in course or gaze stabilization of flies is still unclear [39], both sensory modalities are known to have influences. In our implementation, course stabilization and RotOF cancellation, which can be seen as the counterpart of gaze stabilization, rely only on inertial information.

VIII. Future Work

We are currently integrating an altitude-control system based on an additional OF detector pointing downward and using the same kind of RotOF cancellation as employed for the steering control [1]. Alternative approaches without explicit OF estimation are also being assessed for altitude control [58].

Flying in natural indoor environments is another issue we would like to address. The restricted FOV and constant camera brightness settings employed so far are probably unsuitable for the inhomogeneous lighting and textures of such environments. To tackle this problem, we are developing analog VLSI vision sensors (similar to [57]) with adaptive photoreceptors and built-in OF detection. These chips will provide quick adaptation to ambient light, while being lighter and less energy demanding than the current 1-D cameras. These characteristics are expected to provide a means for reliably detecting OF in more natural environments, and for increasing the FOV covered by the compound eye of our artificial flying insect by using more imaging devices for less weight and power consumption.

Acknowledgment

The authors are grateful to J.-D. Nicoud (http://www.didel.com), A. Guignard, and G. Vaucher for their invaluable support in building the 30-g flying platform. We would like to thank D. Zufferey and C. Ray for their help in constructing the experimental room, and A. Beyeler for his support throughout this project. The authors are equally indebted to the three anonymous reviewers, whose constructive comments have allowed them to significantly improve this paper, and to M. Waibel and C. Cianci who have proofread the manuscript.

References

[1] J. Zufferey and D. Floreano, "Toward 30-gram autonomous indoor aircraft: Vision-based obstacle avoidance and altitude control," in *Proc. IEEE Int. Conf. Robot. Autom.*, Barcelona, Spain, 2005, pp. 2605–2610.

[2] M. Land, "Visual acuity in insects," *Annu. Rev. Entomol.*, vol. 42, pp. 147–177, 1997.

[3] J. Gibson, *The Perception of the Visual World*. Boston, MA: Houghton Mifflin, 1950.

[4] M. Egelhaaf and R. Kern, "Vision in flying insects," *Current Opinion Neurobiol.*, vol. 12, no. 6, pp. 699–706, 2002.

[5] J. Koenderink and A. van Doorn, "Facts on optic flow," *Biol. Cybern.*, vol. 56, pp. 247–254, 1987.

[6] H. Wagner, "Flight performance and visual control of flight of the free-flying housefly (*musca domestica l.*). I. Organization of the flight motor," *Philos. Trans. Roy. Soc. B*, vol. 312, pp. 527–551, 1986.

[7] L. Tammero and M. Dickinson, "The influence of visual landscape on the free flight behavior of the fruit fly *drosophila melanogaster*," *J. Exp. Biol.*, vol. 205, pp. 327–343, 2002.

[8] M. Dickinson, "Haltere-mediated equilibrium reflexes of the fruit fly, *drosophila melanogaster*," *Philos. Trans.: Biol. Sci.*, vol. 354, no. 1385, pp. 903–916, 1999.

[9] G. Nalbach and R. Hengstenberg, "The halteres of the blowfly calliphora—Three-dimensional organization of compensatory reactions to real and simulated rotations," *J. Comparative Physiol. A*, vol. 175, pp. 695–708, 1994.

[10] N. Franceschini, J. Pichon, and C. Blanes, "From insect vision to robot vision," *Philos. Trans. Roy. Soc. B*, vol. 337, pp. 283–294, 1992.

[11] M. Srinivasan, J. Chahl, M. Nagle, and S. Zhang, "Embodying natural vision into machines," in *From Living Eyes to Seeing Machines*, M. Srinivasan and S. Venkatesh, Eds. Oxford, U.K.: Oxford Univ. Press, 1997, pp. 249–265.

[12] A. Duchon, W. H. Warren, and L. Kaelbling, "Ecological robotics," *Adapt. Behav.*, vol. 6, pp. 473–507, 1998.

[13] M. Lewis, "Visual navigation in a robot using zig-zag behavior," in *Neural Information Processing Systems*. Cambridge, MA: MIT Press, 1998, vol. 10.

[14] D. Coombs, M. Herman, T. Hong, and M. Nashman, "Real-time obstacle avoidance using central flow divergence and peripheral flow," in *Proc. 5th Int. Conf. Comput. Vis.*, 1995, pp. 276–283.

[15] J. Santos-Victor, G. Sandini, F. Curotto, and S. Garibaldi, "Divergent stereo for robot navigation: A step forward to a robotic bee," *Int. J. Comput. Vis.*, vol. 14, pp. 159–177, 1995.

[16] K. Weber, S. Venkatesh, and M. Srinivasan, "Insect inspired behaviors for the autonomous control of mobile robots," in *From Living Eyes to Seeing Machines*, M. V. Srinivasan and S. Venkatesh, Eds. Oxford, U.K.: Oxford Univ. Press, 1997, pp. 226–248.

[17] M. Srinivasan, J. Chahl, K. Weber, S. Venkatesh, and H. Zhang, "Robot navigation inspired by principles of insect vision," in *Field and Service Robotics*, A. Zelinsky, Ed. New York: Springer-Verlag, 1998, pp. 12–16.

[18] J. Zufferey, "Bioinspired vision-based flying robots," Ph.D. dissertation, Swiss Federal Inst. Technol. Lausanne (EPFL), Lausanne, Switzerland, 2005.

[19] I. Kroo and P. Kunz, "Mesoscale flight and miniature rotorcraft development," in *Fixed and Flapping Wing Aerodynamics for Micro Air Vehicle Applications*. ser. Progress in Astronautics and Aeronautics, T. J. Mueller, Ed: AIAA, 2001, vol. 195, pp. 503–517.

[20] T. Pornsin-Sirirak, Y.-C. Tai, and C.-M. Ho. Microbat: A palm-sized electrically powered ornithopter. presented at *Proc. NASA/JPL Workshop Biomorphic Robot*. [Online]. Available: http://touch.caltech.edu/publications/2001/jpl/jpl2001.pdf

[21] K. Jones, C. Bradshaw, J. Papadopoulos, and M. Platzer, "Improved performance and control of flapping-wing propelled micro air vehicles," in *Proc. 42nd Aerosp. Sci. Meeting Exhibit.*, Reno, NV, 2004, Paper 2004-0399.
[22] R. Fearing, K. Chiang, M. Dickinson, D. Pick, M. Sitti, and J. Yan, "Wing transmission for a micromechanical flying insect," in *Proc. IEEE Int. Conf. Robot. Autom.*, 2000, pp. 1509–1516.
[23] S. Avadhanula, R. Wood, E. Steltz, J. Yan, and R. Fearing, "Lift force improvements for the micromechanical flying insect," in *Proc. IEEE Int. Conf. Intell. Robots Syst.*, 2003, pp. 1350–1356.
[24] W. Wu, L. Schenato, R. Wood, and R. Fearing, "Biomimetic sensor suite for flight control of a micromechanical flight insect: Design and experimental results," in *Proc. IEEE Int. Conf. Robot. Autom.*, Taipei, Taiwan, R.O.C., 2003, pp. 1146–1151.
[25] L. Schenato, W. Wu, and S. Sastry, "Attitude control for a micromechanical flying insect via sensor output feedback," *IEEE Trans. Robot. Autom.*, vol. 20, no. 1, pp. 93–106, Feb. 2004.
[26] J. Nicoud and J. Zufferey, "Toward indoor flying robots," in *Proc. IEEE/RSJ Int. Conf. Intell. Robots Syst.*, 2002, pp. 787–792.
[27] F. Mura and N. Franceschini, "Visual control of altitude and speed in a flying agent," in *From Animals to Animats III*. Cambridge, MA: MIT Press, 1994, pp. 91–99.
[28] F. Ruffier and N. Franceschini, "Visually guided micro-aerial vehicle: Automatic take off, terrain following, landing and wind reaction," in *Proc. IEEE Int. Conf. Robot. Autom.*, T. J. Tarn, T. Fukuda, and K. Valavanis, Eds., New Orleans, LA, Apr. 2004, pp. 2339–2346.
[29] J. Chahl, M. Srinivasan, and H. Zhang, "Landing strategies in honeybees and applications to uninhabited airborne vehicles," *Int. J. Robot. Res.*, vol. 23, no. 2, pp. 101–1102, 2004.
[30] T. Neumann and H. Bülthoff, "Behavior-oriented vision for biomimetic flight control," in *Proc. EPSRC/BBSRC Int. Workshop Biol. Inspired Robot.*, 2002, pp. 196–203.
[31] L. Muratet, S. Doncieux, Y. Brière, and J.-A. Meyer, "A contribution to vision-based autonomous helicopter flight in urban environments," *Robot. Auton. Syst.*, to be published.
[32] M. Reiser and M. Dickinson, "A test bed for insect-inspired robotic control," *Philos. Trans.: Math., Phys., Eng. Sci.*, vol. 361, pp. 2267–2285, 2003.
[33] G. Barrows and C. Neely, "Mixed-mode VLSI optic flow sensors for in-flight control of a micro air vehicle," *Critical Technol. Future Comput., SPIE*, vol. 4109, pp. 52–63, 2000.
[34] G. Barrows, C. Neely, and K. Miller, "Optic flow sensors for MAV navigation," in *Fixed and Flapping Wing Aerodynamics for Micro Air Vehicle Applications*. ser. Progress in Astronautics and Aeronautics, T. J. Mueller, Ed: AIAA, 2001, vol. 195, pp. 557–574.
[35] W. Green, P. Oh, K. Sevcik, and G. Barrows, "Autonomous landing for indoor flying robots using optic flow," in *Proc. ASME Int. Mech. Eng. Congr. Expo.*, vol. 2, 2003, pp. 1347–1352.
[36] P. Oh, W. Green, and G. Barrows, "Closed quarter aerial robot prototype to fly in and around buildings," in *Proc. Int. Conf. Comput., Commun., Control Technol.*, vol. 5, 2003, pp. 302–307.
[37] W. Green, P. Oh, and G. Barrows, "Flying insect inspired vision for autonomous aerial robot maneuvers in near-earth environments," in *Proc. IEEE Int. Conf. Robot. Autom.*, vol. 3, 2004, pp. 2347–2352.
[38] R. Nelson and Y. Aloimonos, "Finding motion parameters from spherical flow fields (or the advantages of having eyes in the back of your head)," *Biol. Cybern.*, vol. 58, pp. 261–273, 1988.
[39] H. Krapp, "Neuronal matched filters for optic flow processing in flying insects," in *Neuronal Processing of Optic Flow*, M. Lappe, Ed. San Diego, CA: Accademic, 2000, pp. 93–120.
[40] J. Zufferey, A. Beyeler, and D. Floreano, "Vision-based navigation from wheels to wings," in *Proc. IEEE/RSJ Int. Conf. Intell. Robots Syst.*, vol. 3, 2003, pp. 2968–2973.
[41] M. Srinivasan, "An image-interpolation technique for the computation of optic flow and egomotion," *Biol. Cybern.*, vol. 71, pp. 401–416, 1994.
[42] B. Horn, *Robot Vision*. Cambridge, MA: MIT Press, 1986.
[43] N. Ancona and T. Poggio, "Optical flow from 1D correlation: Application to a simple time-to-crash detector," in *Proc. 4th Int. Conf. Comput. Vis.*, 1993, pp. 209–214.
[44] T. Poggio, A. Verri, and V. Torre, "Green theorems and qualitative properties of the optical flow," Mass. Inst. Technol., Cambridge, MA, Tech. Rep. A.I. Memo 1289, 1991.
[45] D. Lee, "A theory of visual control of braking based on information about time-to-collision," *Perception*, vol. 5, pp. 437–459, 1976.
[46] T. Camus, "Calculating time-to-contact using real-time quantized optical flow," Nat. Inst. Standards Technol., Tech. Rep. 5609, 1995.
[47] M. Srinivasan, S. Zhang, M. Lehrer, and T. Collett, "Honeybee navigation en route to the goal: Visual flight control and odometry," *J. Exp. Biol.*, vol. 199, pp. 237–244, 1996.
[48] A. Borst, "How do flies land? From behavior to neuronal circuits," *BioSci.*, vol. 40, no. 4, pp. 292–299, 1990.
[49] R. Brooks, *Cambrian Intelligence*. Cambridge, MA: The MIT Press, 1999.
[50] R. Hengstenberg, "Gaze control in the blowfly calliphora: A multisensory two-stage integration process," *Neurosci.*, vol. 3, pp. 19–29, 1991.
[51] W. Reichardt, "Movement perception in insects," in *Processing of Optical Data by Organizms and by Machines*, W. Reichardt, Ed. New York: Academic, 1969, pp. 465–493.
[52] M. Srinivasan, M. Poteser, and K. Kral, "Motion detection in insect orientation and navigation," *Vis. Res.*, vol. 39, no. 16, pp. 2749–2766, 1999.
[53] L. Tammero and M. Dickinson, "Collision-avoidance and landing responses are mediated by separate pathways in the fruit fly," *J. Exp. Biol.*, vol. 205, pp. 2785–2798, 2002.
[54] M. Srinivasan, S. Zhang, J. Chahl, E. Barth, and S. Venkatesh, "How honeybees make grazing landings on flat surfaces," *Biol. Cybern.*, vol. 83, pp. 171–183, 2000.
[55] N. Franceschini, "From fly vision to robot vision: Reconstruction as a mode of discovery," in *Sensors and Sensing in Biology and Engineering*, F. G. Barth, J. A. Humphrey, and T. W. Secomb, Eds. New York: Springer, 2003, pp. 223–235.
[56] A. Sherman and M. Dickinson, "Summation of visual and mechanosensory feedback in *drosophila* flight control," *J. Exp. Biol.*, vol. 207, pp. 133–142, 2004.
[57] J. Kramer, R. Sarpeshkar, and C. Koch, "An analog VLSI velocity sensor," in *Proc. IEEE Int. Symp. Circuits Syst.*, 1995, pp. 413–416.
[58] A. Beyeler, C. Mattiusi, J. Zufferey, and D. Floreano, "Vision-based altitude and pitch estimation for ultralight indoor aircraft," in *Proc. IEEE Int. Conf. Robot. Autom.*, to be published.

Jean-Christophe Zufferey (M'05) completed his master project at Carnegie Mellon University, Pittsburgh, PA, as an exchange student, and he received the M.S. degree in microengineering in 2001. In 2005, he received the Ph.D. degree in autonomous robotics.

He is currently a Research Scientist with the Swiss Federal Institute of Technology in Lausanne (EPFL), Lausanne, Switzerland, in the Laboratory of Intelligent Systems. His research interests are in aerial, bioinspired, and evolutionary robotics. He has coauthored eight peer-reviewed journal and conference papers. He is also Co-Founder of an EPFL spin-off company, DIDEL, which is involved in educational robotics and ultralight indoor slow-flyers.

Dario Floreano (M'96) is currently an Associate Professor of Intelligent Systems at the Swiss Federal Institute of Technology in Lausanne (EPFL), Lausanne, Switzerland, where he is also Director of the Laboratory of Intelligent Systems and of the Institute of Systems Engineering. His research activities span bioinspired and evolutionary robotics, biomimetic electronics, neural computation, self-organizing systems, and biology reverse engineering.

He has published more than 100 peer-reviewed papers, authored two books, and edited three other books. The book *Evolutionary Robotics* was reprinted by MIT Press three times over the last four years. He co-organized eight international conferences, and joined the program committee of more than 70 other conferences. He is on the editorial board of eight international journals: *Neural Networks*, *Genetic Programming and Evolvable Machines*, *Adaptive Behavior*, *Artificial Life*, *Connection Science*, *Evolutionary Computation*, the IEEE TRANSACTIONS ON EVOLUTIONARY COMPUTATION, and *Autonomous Robots*. He is cofounder and member of the Board of Directors of the International Society for Artificial Life, Inc., and a member of the Board of Governors of the International Society for Neural Networks.